

The analysis of the impact of fear in the presence of additional food and prey refuge with nonlocal predator-prey models

Sangeeta Saha^a, Swadesh Pal^{a,*}, Roderick Melnik^{a,b}

^a*MS2 Discovery Interdisciplinary Research Institute, Wilfrid Laurier University, Waterloo, Canada*

^b*BCAM - Basque Center for Applied Mathematics, E-48009, Bilbao, Spain*

Abstract

In a predator-prey interaction, many factors are present that affect the growth of the species, either positively or negatively. Fear of predation is such a factor that causes psychological stress in a prey species, so their overall growth starts to decline. In this work, a predator-prey model is proposed where the prey species faces a reduction in their growth out of fear, and the predator is also provided with an alternative food source that helps the prey to hide in a safer place. The dynamics produce a wide range of interesting results, including the significance of the presence of a certain amount of fear or even prey refuge for population coexistence. The analysis is extended later to the nonlocal model to analyze how the non-equilibrium phenomena influence the dynamical behaviour. It is observed through numerical simulations that the scope of pattern formation reduces with the increase of fear level in the spatio-temporal model, whereas the incorporation of nonlocal interaction further increases the chance of species colonization.

Keywords: Additional food, Psychological effects, Nonlocal model, Bio-social dynamics, Turing instability

1. Introduction

The essential component in ecology is the interaction between predators and their prey, as this upholds the biomass flow from one trophic level to others and maintains the population size. Researchers have developed several mathematical models to explore the dynamic nature, such as predators searching for prey for survival, prey adopting different strategies to avoid higher predation, etc. This paper considers a predator-prey model where the growth of a prey species is affected by its predator along with their spatial local and nonlocal interactions.

In an ecosystem, a predator can have a direct, indirect, or combined impact on their prey. For example, they have an immediate impact when consuming a prey species. Besides that, they can also have an indirect or non-consumption effect by making the prey population afraid and compelling them to adjust their behaviour accordingly [1]. As the prey species are constantly concerned about a potential attack, the fear effect of predators mainly reflects continuous psychological stress. In fact, when direct predation is absent, the fear effect sometimes has a stronger impact on prey reduction or even prey extinction. Hunting and reproduction are two significant behaviours of prey that can alter due to fear [2]. In every taxon, all animals respond to the predation risk and show a variety of anti-predator responses, which include habitat changes, foraging, vigilance, and different physiological changes [3–5]. Due to fear of

*Corresponding author

Email addresses: sangeetasaha629@gmail.com (Sangeeta Saha), spa1@wlu.ca (Swadesh Pal), rmelnik@wlu.ca (Roderick Melnik)

predation risk, the prey population can change its grazing zone to a safer place and tries to search for food at those places where predation risk is low, yet food is more readily available [6, 7]. Furthermore, they try to increase their vigilance, adjust their reproductive strategies, etc. These anti-predator behaviours are beneficial as a short-term survival strategy by increasing adult survivability, but they can reduce reproduction as a long-term cost [3].

Recently, researchers have focused on pursuing their studies on how indirect methods become more effective than direct killing in reducing prey populations [2, 8, 9]. It has been observed that the reproduction of song sparrows was affected by the fear effect of their predators (raccoon, owl, hawk, etc.) during the entire breeding season, even if the direct predation is excluded [2]. There were fewer eggs, hatchlings, and even fledglings in the next generation, and the reproduction rate decreased by about 40%. An experiment on free-living wild songbird populations shows that in the presence of predator playback, songbird parents generated 53% fewer recruits to the adult breeding population [10]. On the other hand, parental behaviours of pumpkinseed (*Lepomis gibbosus*), including in-nest rotations and egg and nest maintenance, are altered because of their avian predator, the Osprey (*Pandion haliaetus*) [11]. Moreover, mesocarnivores (raccoons) reduce their foraging activities by 66% due to the fear of large carnivores (cougar, wolf, black bear) [8]. In the aquatic environment, it is observed that the normal growth rate of bluegill can rise by almost 27% when predators, including largemouth bass, trout, turtles, etc., are absent [12]. Furthermore, there are several predator-prey interactions where the reproduction of the scared prey decreases due to fear of predation risk, e.g., bluebirds-avian predators [13], elk-wolves [14, 15], snowshoe hares-dogs [16], dugongs-sharks [15], mule deer-mountain lions [17], etc. Research has shown that the anxiousness of a predator alone may alter a prey's behaviour. Wang et al. first included fear of the predator on a prey species in their model by lowering the prey's birth rate [9]. They noticed that the system's oscillation may be stabilized by the fear effect. Several research works have already been conducted to explore how this fear of predation makes an impact on the dynamic behaviour of predator-prey interactions [18–20], tri-trophic food chain models [21, 22], ecological models with prey refuge [23], stage-structured models [24], spatio-temporal models [25], etc.

The essential component, known as the functional response, is used to represent the behavioural traits of the predator species. There are different types of predator-prey interactions, and how the predator consumes their prey affects the dynamic behaviour to a greater extent. There are several factors that affect the functional responses, including the biomass of the prey, the predators' effectiveness in finding, handling, and killing the prey, their competition, etc. The most used prey-dependent functional responses are Lotka–Volterra type and Holling-type responses [26]. However, in many scenarios, the functional response in a predator-prey framework should be predator-dependent, particularly when predators need to look for food (share or compete for it). According to a wide range of literature, predator dependency in the functional response appears to be common in both natural systems and laboratory settings [27, 28]. Numerous studies and observations imply that prey changes behaviour because of increased predator risk, and predators interfere with one another's activities to create competitive effects. This interference may occur because of inadequate prey biomass, unfavourable environment, or territorial disputes [29]. To mediate between theoretical and experimental viewpoints, Beddington [30] and DeAngelis et al. [31] independently suggested a functional response considering the mutual interference amongst predators. It is assumed that two or more predator populations spend some time interfering with one another's actions except when searching for and processing the prey species. In addition, the influence of predator interference on the feeding rate decreases with prey quantity, indicating that predators' collective behaviour becomes less significant.

There are several cases where fear affects the prey growth rate. For instance, the predator

depends only on this targeted prey species, and then the prey species restricts its growth, which causes the predator to look for other food sources to survive. So, an additional food in the predator population solves this dilemma. Now, the additional/alternative food can be provided in two ways. First, if a predator is given extra food, it can divert their attention away from the prey, lowering the predation rate. It helps the predator species to grow at a higher rate, which will be beneficial in controlling the oscillations of the predator-prey system. During this time, the predator will be busy dealing with this additional/alternative food, and the targeted prey species will manage to move towards some safe zones, creating prey refuge and will be able to save themselves from extinction. It is observed in an experiment that when a sufficient amount of additional food was given to hen harriers during their trial, the predation rate decreased from 3.7 chicks per 100 hours to 0.5 chicks per 100 hours [32]. Secondly, if a predator is given more food sources, it may become more vigilant or elevate the reproduction rate. This situation anticipates a rise in predator-prey interactions, resulting in a reduction or even extinction of prey species. Crawley has shown that when assessing the effects of additional food for predators on a dynamic system, the factors of “quality” and “quantity” of the food play a key role [33]. Several studies state that good quality extra food sources result in high predation rates, whereas low quality may conserve the target prey [34, 35]. As the predators are given more food, it will preserve the ecological balance and prevent the overuse of prey resources.

The homogeneous distribution throughout the spatial domain is an assumption made by the temporal models of interacting populations. However, it is hard to correctly model the random movement of individuals across the short or long-range without taking spatio-temporal models into account. The emergence of spatio-temporal patterns in predator-prey interactions stemming from the reaction-diffusion equation has garnered significant interest since Alan Turing’s pioneering research on chemical morphogenesis [36]. The kinetics of the reaction plays an important role in developing different kinds of stationary and non-stationary spatial patterns. The reaction-diffusion systems may also be used to explain models of ecological invasions [37], the spread of diseases [38], etc. Researchers have extensively examined the spatio-temporal pattern formation in reaction-diffusion models and have identified several mechanisms, including Hopf bifurcation [39], diffusion-driven instabilities (Turing instability) [40], etc. Non-stationary spatial patterns among these comprise spatio-temporal chaotic patterns, periodic travelling waves, and travelling waves. The population patches never settle down to any stationary distribution due to these later patterns, which continue to change over time. Most stationary patterns are seen when the parameter values are chosen from the Turing or Turing-Hopf domain. Non-stationary spatial patterns, such as travelling waves, modulated travelling waves, etc., are also seen for a specific range of parameter values not connected to Turing instability.

The spatio-temporal local models are formulated based on the assumption that individuals at a given spatial point interact with one other only and that members of both species can move between spatial points. However, this kind of equation with local interaction can not model the situation in which an individual placed at one spatial position can access resources located at another spatial point. Some published works incorporate nonlocal interaction factors into the reaction kinetics to describe such scenarios [41–44]. In a nonlocal predator-prey interaction, individuals at a spatial position can migrate to a different place to use the resources located at that location [42]. It was observed that the system produces a spatio-temporal chaotic pattern for a large consumption rate when the predator starts to move to a nearby location in the presence of abundant prey. In addition, the same model with local interaction does not produce any Turing pattern, but the nonlocal model does. Depending on the range of the nonlocal interaction, the nonlocal model produces patches of different widths, and periodic time oscillation is replaced by a stationary non-homogeneous distribution [41].

Our main intention in this work is to explore the impact of psychological effects affecting

predator-prey interactions in terms of fear of predation through a local and nonlocal approach. Here, a predator-prey relationship is presented, in which the fear of the predators affects the prey's reproduction, and the predators interfere in their activities during prey consumption. In this case, there is an indirect psychology that works among predators to get more food. In addition, the prey species has a tendency to move towards a predator-free zone in the absence of fear. Furthermore, we have explored how the nonlocal fear term affects the overall dynamic behaviour. We have revealed several results, such as the fear of predation affecting the coexistence of the species in an environment, the influence of other psychological factors, including intra-specific competition and prey refuge on the population, etc. Nevertheless, we have shown that the nonlocal fear term positively impacts species migration.

2. Model Formulation

The environment mainly consists of food webs and corresponding food chains, which are nothing but predator-prey interactions. Many factors present in our surroundings contribute positively or negatively to the growth of a species. In this work, we are dealing with a predator-prey interaction where some psychological aspects for both species have been considered. Wang et al., in 2016, have proposed a predator-prey model where the growth rate of prey is reduced because of the fear of predation [9]. The model they have proposed is given as:

$$\begin{aligned}\frac{du}{dt} &= ru\bar{f}_1(\omega, v) - du - pu^2 - \bar{f}_2(u)v, \quad u(0) > 0, \\ \frac{dv}{dt} &= v(-\mu_1 + c\bar{f}_2(u)), \quad v(0) > 0,\end{aligned}\tag{2.1}$$

where ω defines the level of fear that drives the anti-predator behaviour of prey, and the function $\bar{f}_1(\omega, v) = 1/(1 + \omega v)$ satisfies the following conditions:

$$\begin{aligned}(i) \bar{f}_1(\omega, 0) &= 1, & (ii) \bar{f}_1(0, v) &= 1 & (iii) \lim_{\omega \rightarrow \infty} \bar{f}_1(\omega, v) &= 0, & (iv) \lim_{v \rightarrow \infty} \bar{f}_1(\omega, v) &= 0, \\ (v) \frac{\partial \bar{f}_1}{\partial \omega} &< 0, & (vi) \frac{\partial \bar{f}_1}{\partial v} &< 0.\end{aligned}$$

The prey and predator biomass are denoted by u and v , respectively. The intrinsic growth rate of prey species is r , and the parameter d is their natural death rate. The prey is involved in intra-specific competition at rate p . Lastly, $\bar{f}_2(u)$ denotes the prey-dependent functional response, and μ_1 is the natural mortality rate of predator. Though they have considered only prey-dependent functional response, there is literature stating that the predators affect each other's activities when they become large in number compared to the available prey biomass [29]. In this work, we have chosen a predator-dependent functional response, named the Beddington-DeAngelis response, where it is considered that the predator species spend some time encountering each other except searching for and processing the prey. The predator-prey interaction stated in (2.1) with Beddington-DeAngelis functional response takes the form [19, 22]:

$$\begin{aligned}\frac{du}{dt} &= ru\bar{f}_1(\omega, v) - du - pu^2 - \frac{auv}{b + u + lv}, \quad u(0) > 0, \\ \frac{dv}{dt} &= v \left(-\mu_1 + \frac{cau}{b + u + lv} \right), \quad v(0) > 0.\end{aligned}\tag{2.2}$$

Let us consider t_u and t_v as the handling times of the predator per prey and interaction time between two or more predators. Then, the maximum predation rate will be $a = 1/t_u$. Moreover, the parameters e_u and e_v are the constants that signify the rate of the predator's movement

to detect a prey and another predator, respectively [45]. Then the parameter $b = 1/(e_u t_u)$ denotes the normalization coefficient relating the prey and predator biomass to their interacting environment [31]. Here, c is a quantity from $(0, 1)$ that represents the positive contribution of the food consumed by the predator, converted into predator biomass, which makes ‘ ca ’ the maximum growth of predator species. And lastly, as we have considered the predator’s interference at the time of consumption, the parameter l looks like $l = (e_v t_v)/(e_u t_u)$. Moreover, a predator species usually does not depend only on one particular prey, so let us assume an additional/alternative food source of biomass A is uniformly distributed to the habitat where the predator and prey interact. It is considered that the amount of additional food is proportional to the number of encounters the predator is having with additional food. In this case, the model becomes

$$\begin{aligned} \frac{du}{dt} &= ru\bar{f}_1(\omega, v) - du - pu^2 - \frac{auv}{b + \alpha\eta A + u + lv}, \quad u(0) > 0, \\ \frac{dv}{dt} &= v \left(-\mu_1 + \frac{ca(u + \eta A)}{b + \alpha\eta A + u + lv} \right), \quad v(0) > 0. \end{aligned} \quad (2.3)$$

The model (2.3) is a predator-prey interaction where the growth rate of prey species is affected by fear of predators, additional food is provided to predators, and the predators follow Beddington-DeAngelis functional response towards available food. The parameter $\alpha = t_A/t_u$ signifies the quality of additional food compared to the prey species if t_A is chosen to be the time taken by the predator to handle per unit of additional food. Also, if e_A is considered as the constant representing the rate of movement of the predator at the time of searching to detect the alternative food source, then $\eta = e_A/e_u$ represents the effectual ability of the predator species to detect the additional food. It means ηA is the quantity of additional food the predator can notice relative to the prey species.

When the predator spends time searching and handling alternative food sources, the targeted prey can successfully hide in places that are not accessible to the predator, creating a prey refuge. Here, it is considered that m is the fraction of prey hiding, which leaves $(1 - m)$ portion of prey provided to the predator. Now, if many predators are exposed to prey species that are inadequate in the environment, they become involved in intra-specific competition. Gaining more food becomes the priority in such a scenario. We have considered parameter μ_2 as the intra-specific competition rate of predator species. Hence, summing up all the assumptions, we finally propose the temporal model in (2.4) as follows:

$$\begin{aligned} \frac{du}{dt} &= \frac{ru}{1 + \omega v} - du - pu^2 - \frac{a(1 - m)uv}{b + \alpha\eta A + (1 - m)u + lv} \equiv \frac{ru}{1 + \omega v} - uf_1(u, v), \\ \frac{dv}{dt} &= \frac{ca\{(1 - m)u + \eta A\}v}{b + \alpha\eta A + (1 - m)u + lv} - \mu_1 v - \mu_2 v^2 \equiv vf_2(u, v), \end{aligned} \quad (2.4)$$

with non-negative initial conditions. The system parameters are chosen to be positive along with $r > d$.

2.1. Local spatio-temporal model

The distributions of populations are generally heterogeneous and depend on time and the spatial positions in the habitat. So, it is natural and more precise to study the corresponding PDE problem. In this work, we have considered the spatio-temporal model with reaction kinetics of system (2.4) in a bounded domain $\Omega \subset \mathbb{R}$ with closed boundary $\partial\Omega$ and $\bar{\Omega} = \Omega \cup \partial\Omega$

as:

$$\begin{aligned}\frac{\partial u}{\partial t} &= d_1 \frac{\partial^2 u}{\partial x^2} + \frac{ru}{1 + \omega v} - du - pu^2 - \frac{a(1-m)uv}{b + \alpha\eta A + (1-m)u + lv}, \\ \frac{\partial v}{\partial t} &= d_2 \frac{\partial^2 v}{\partial x^2} + \frac{ca\{(1-m)u + \eta A\}v}{b + \alpha\eta A + (1-m)u + lv} - \mu_1 v - \mu_2 v^2,\end{aligned}\tag{2.5}$$

subject to non-negative initial conditions, and to make the model simple, we have chosen periodic boundary conditions. There is not much qualitative change in the dynamics of the nonlocal model by changing the boundary conditions periodic to no-flux [46]. Here, the parameters d_1 and d_2 represent the diffusion coefficients corresponding to prey and predator species.

2.2. Nonlocal interaction

The model (2.5) assumes that the predator located at the space point x impacts the growth of prey at the same point. However, in reality, the fear of predators at a spatial location x depends not only on the local appearance of the predator but also on the predator density in other nearby points, i.e., a prey located at space point x can be scared by those predators who are located in some areas around this spatial point, and it can be obtained by convolution term

$$U(x, t) = (\phi_\delta * v)(x, t) = \int_{-\infty}^{\infty} \phi_\delta(x - y)v(y, t)dy.$$

Here, the kernel function $\phi_\delta(y)$ describes the impact of fear on prey at the space point x by the predator at the space point y . Hence, the kernel ϕ_δ is a function dependent on the position x . The first subscript δ is the range of nonlocal interaction. We assume the kernel function ϕ_δ to be non-negative with compact support. Also, to preserve the same homogeneous steady-state solutions for both the local and nonlocal models, we assume that $\int_{-\infty}^{\infty} \phi_\delta(y)dy = 1$. The impact of fear on prey is limited by the number of predators they are facing or encountering. We can apply this limitation to each space point independently. This means that predators located at space point y make an impact on prey at space point x_1 independently of its concentration at another point x_2 . Considering the work of Furter and Grinfeld [47] and using the aforementioned assumption, we obtain the rate of impact of fear on prey at the space point x as

$$M(x, t) = \frac{ru}{1 + \omega(\phi_\delta * v)} = \frac{ru(x, t)}{1 + \omega \int_{-\infty}^{\infty} \phi(x - y)v(y, t)dy}.$$

Implementing the nonlocal fear term of prey species as well as the random motion of the population, we get the integro-differential equation model as

$$\begin{aligned}\frac{\partial u}{\partial t} &= d_1 \frac{\partial^2 u}{\partial x^2} + \frac{ru}{1 + \omega(\phi_\delta * v)} - du - pu^2 - \frac{a(1-m)uv}{b + \alpha\eta A + (1-m)u + lv}, \\ \frac{\partial v}{\partial t} &= d_2 \frac{\partial^2 v}{\partial x^2} + \frac{ca\{(1-m)u + \eta A\}v}{b + \alpha\eta A + (1-m)u + lv} - \mu_1 v - \mu_2 v^2,\end{aligned}\tag{2.6}$$

with non-negative initial conditions and periodic boundary conditions.

3. Analysis of the Proposed Systems

It is important to show that the proposed system is biologically well-defined, and for this, we need to check the positivity and uniform boundedness of the system variables. The following theorem states that the model (2.4) is well-posed, and its proof is given in Appendix A.1.

Theorem 3.1. *Solutions of system (2.4), starting in \mathbb{R}_+^2 , are non-negative for $t > 0$ and uniformly bounded provided $r > d$.*

3.1. Equilibrium points for the temporal model and their stabilities

The temporal model (2.4) has

- (i) a trivial equilibrium point $E_0 = (0, 0)$;
- (ii) two planer equilibrium points $E_1 = (\bar{u}, 0) \equiv \left(\frac{r-d}{p}, 0\right)$ and $E_2 = (0, \tilde{v})$ where \tilde{v} is the root of the equation

$$\mu_2 lv^2 + (\mu_1 l + \mu_2 s)v - (ca\eta A - \mu_1 s) = 0, \text{ where } s = b + \alpha\eta A.$$

Here, the feasibility of the equilibrium point E_2 depends on the condition $ca\eta A > \mu_1 s$;

- (iii) the coexisting equilibrium point $E^* = (u^*, v^*)$, where

$$u^* = \frac{(s + lv^*)(\mu_1 + \mu_2 v^*) - ca\eta A}{(1 - m)[ca - (\mu_1 + \mu_2 v^*)]}$$

and v^* is the root of the following equation

$$B_1 v^4 + B_2 v^3 + B_3 v^2 + B_4 v + B_5 = 0, \quad (3.1)$$

with $B_1 = a\omega\mu_2[cp l^2 + \mu_2(1 - m)^2] > 0$, $B_2 = a\mu_2(1 - m)^2(\mu_2 - 2\omega A_1) + cal[p\mu_2(l + \omega A_4) + \omega\{pA_3 - d\mu_2(1 - m)\}]$, $B_3 = ca[l\mu_2\{pA_4 + r(1 - m)\} + (l + \omega A_4)\{pA_3 - d\mu_2(1 - m)\} + \omega l\{pA_2 + d(1 - m)A_1\}] + a(1 - m)^2(ca - \mu_1)\{\omega(ca - \mu_1) - 2\mu_2\}$, $B_4 = ca[A_4\{pA_3 + \mu_2(r - d)(1 - m)\} + (l + \omega A_4)\{pA_2 + d(1 - m)A_1\} - rl(1 - m)A_1] + a(1 - m)^2 A_1^2$, $B_5 = caA_4\{pA_2 - (r - d)(1 - m)A_1\}$, $A_1 = ca - \mu_1$, $A_2 = \mu_1 s - ca\eta A$, $A_3 = s\mu_2 + l\mu_1$, and $A_4 = s - \eta A$.

Here, $B_1 > 0$ holds always. So, the number of positive v^* will depend on the signs of coefficients B_i , for $i = 2, 3, 4, 5$. For example, equation (3.1) will not possess any feasible v^* if $B_i > 0$, for $i = 2, \dots, 5$, but can have at most four positive roots if $B_2, B_4 < 0$ and $B_3, B_5 > 0$ hold. Moreover, equation (3.1) has at least one positive root if any of the following conditions hold: (i) $B_i > 0$, $i = 2, 3, 4$ and $B_5 < 0$; (ii) $B_i > 0$, $i = 2, 3$ and $B_j < 0$, $j = 4, 5$; (iii) $B_2 > 0$ and $B_i < 0$, $i = 3, 4, 5$; (iv) $B_i < 0$, $i = 2, \dots, 5$.

Furthermore, if $ca > (\mu_1 + \mu_2 v^*)$ holds along with positive v^* , then $u^* > 0$ when $(s + lv^*)(\mu_1 + \mu_2 v^*) > ca\eta A$ is satisfied. On the other hand, if $ca < (\mu_1 + \mu_2 v^*)$ holds with $v^* > 0$, then $(s + lv^*)(\mu_1 + \mu_2 v^*) < ca\eta A$ has to be fulfilled for the feasibility of u^* .

Now, we discuss the local stability criterion of the equilibrium points, which can be determined by analyzing the eigenvalues of corresponding Jacobian matrices. Let us denote $s = b + \alpha\eta A$. The Jacobian matrix of system (2.4) is

$$\mathbf{J} = \begin{pmatrix} a_{11} & a_{12} \\ a_{21} & a_{22} \end{pmatrix}, \quad (3.2)$$

where $a_{11} = \frac{r}{1+\omega v} - \frac{a(1-m)v(s+lv)}{\{s+(1-m)u+lv\}^2} - d - 2pu$, $a_{12} = -\frac{r\omega u}{(1+\omega v)^2} - \frac{a(1-m)u\{s+(1-m)u\}}{\{s+(1-m)u+lv\}^2}$, $a_{21} = \frac{ca(1-m)v\{b+lv+\eta A(\alpha-1)\}}{\{s+(1-m)u+lv\}^2}$ and $a_{22} = \frac{ca\{(1-m)u+\eta A\}\{s+(1-m)u\}}{\{s+(1-m)u+lv\}^2} - \mu_1 - 2\mu_2 v$.

The following theorem states the local stability property of the boundary equilibrium and interior equilibrium points, and its proof is illustrated in Appendix A.2.

Theorem 3.2. *System (2.4) has several axial and interior equilibrium points, among which*

- (a) E_0 is an unstable equilibrium point.
- (b) E_1 is locally asymptotically stable when $(ca - \mu_1)(1 - m)\bar{u} < \mu_1 s - ca\eta A$ holds.
- (c) E_2 is locally asymptotically stable when $\omega\{dl + a(1 - m)\}\tilde{v}^2 + \{ds\omega + a(1 - m) - (r - d)l\}\tilde{v} - (r - d)s > 0$ holds.

- (d) E^* is locally asymptotically stable if the following two conditions hold, i.e.,
- (i) $av^*[(1-m)^2u^* - lc(1-m)u^* - lc\eta A] < (pu^* + \mu_2v^*)K^2$,
 - (ii) $p\mu_2K^4 + [ca\{pl\{(1-m)u^* + \eta A\} + r\omega(1-m)\{b + lv^* + \eta A(\alpha - 1)\}\} - a\mu_2(1-m)^2v^*]K^2 + ca^2(1-m)^2[\{s + (1-m)u^*\}\{b + lv^* + \eta A(\alpha - 1)\} + (s - \eta A)lv^*] > 0$,
- where $K = [s + (1-m)u^* + lv^*] > 0$.

3.2. Local bifurcations for the temporal model

The local bifurcations around the equilibrium points are analyzed mainly with the help of Sotomayor's theorem and Hopf's bifurcation theorem [48]. For instance, if the stability condition of any of the equilibrium points in the system violates in such a way that the corresponding determinant becomes 0, giving a simple zero eigenvalue, then there will occur transcritical bifurcation, and we can observe the exchange of stability in that bifurcation threshold. The following theorems will state the conditions where such bifurcation can be observed for E_1 and E_2 .

Theorem 3.3. *Choosing a as the bifurcating parameter, system (2.4) undergo transcritical bifurcations around*

- (i) $E_1(\bar{u}, 0)$ at $a_{[TC_1]} = [\mu_1\{s + (1-m)\bar{u}\}]/[c\{\eta A + (1-m)\bar{u}\}]$.
- (ii) $E_2(0, \tilde{v})$ at $a = a_{[TC_2]}$, where $a_{[TC_2]}$ is the positive root of the equation $\omega\{dl + a(1-m)\}\tilde{v}^2 + \{dsw + a(1-m) - (r-d)l\}\tilde{v} - (r-d)s = 0$.

On the other hand, if any of the mentioned inequalities in (A.2) is violated, then the equilibrium point becomes unstable, and the system performs oscillatory or non-oscillatory behaviour. The system starts to oscillate around (u^*, v^*) if $F_1 > 0$ along with $F_1^2 - 4F_2 < 0$ as the eigenvalues will be in the form of the complex conjugate in this case. So, we get the following theorem:

Theorem 3.4. *Suppose E^* exists with the feasibility conditions. A simple Hopf bifurcation occurs at unique $\omega = \omega_{[H]}$ around E^* , where $\omega_{[H]}$ is the positive root of $F_1(\omega) = 0$ providing $F_2(\omega_{[H]}) > 0$ (stated in equation (A.1)).*

The proofs of both Theorems 3.3 and 3.4 are elaborated in Appendix A.3.

3.3. Turing instability analysis for the local and nonlocal models

We intend to find the condition for Turing instability. If the homogeneous steady state of the temporal model is locally stable to infinitesimal perturbation but becomes unstable in the presence of diffusion, a scenario of Turing instability occurs. For the temporal model, $E^*(u^*, v^*)$ is locally asymptotically stable when $F_1 = -(a_{11} + a_{22}) > 0$ and $F_2 = a_{11}a_{22} - a_{12}a_{21}$ hold. Here, we apply heterogeneous perturbation around E^* to obtain the criterion for instability of the spatio-temporal model. Let us perturb the homogeneous steady state of the local system (2.5) around (u^*, v^*) by

$$\begin{pmatrix} u \\ v \end{pmatrix} = \begin{pmatrix} u^* \\ v^* \end{pmatrix} + \epsilon \begin{pmatrix} u_1 \\ v_1 \end{pmatrix} e^{\lambda t + ikx}$$

with $|\epsilon| \ll 1$ where λ is the growth rate of perturbation and k denotes the wave number. Substituting these values in system (2.5), the linearization takes the form:

$$\mathbf{J}_k \begin{bmatrix} u_1 \\ v_1 \end{bmatrix} \equiv \begin{bmatrix} a_{11} - d_1k^2 - \lambda & a_{12} \\ a_{21} & a_{22} - d_2k^2 - \lambda \end{bmatrix} \begin{bmatrix} u_1 \\ v_1 \end{bmatrix} = \begin{bmatrix} 0 \\ 0 \end{bmatrix}, \quad (3.3)$$

where a_{11} , a_{12} , a_{21} and a_{22} are mentioned in the proof of Theorem 3.2. We are interested in finding the non-trivial solution of the system (3.3), so λ must be a zero of $\det(\mathbf{J}_k) = 0$, where \mathbf{J}_k is the coefficient matrix of the system (3.3). Now

$$\det(\mathbf{J}_k) = \lambda^2 - B(k^2)\lambda + C(k^2)$$

with $B(k^2) = \text{tr}(\mathbf{J}(E^*)) - (d_1 + d_2)k^2$, $C(k^2) = \det(\mathbf{J}(E^*)) - (d_2a_{11} + d_1a_{22})k^2 + d_1d_2k^4$. So, $\det(\mathbf{J}_k) = 0$ gives

$$\lambda_{\pm}(k^2) = \frac{B(k^2) \pm \sqrt{(B(k^2))^2 - 4C(k^2)}}{2}$$

The Turing instability conditions are given as

$$(i) a_{11} + a_{22} < 0, (ii) a_{11}a_{22} > a_{12}a_{21}, \text{ and } (iii) d_2a_{11} + d_1a_{22} > 2\sqrt{d_1d_2(a_{11}a_{22} - a_{12}a_{21})}.$$

Here $B(k^2) < 0$ for all k when the temporal model is locally asymptotically stable. So, the homogeneous solution will be stable under heterogeneous perturbation when $C(k^2) > 0$ for all k . The system is unstable if the inequality is violated for some $k \neq 0$.

Here $k_{min}^2 = (d_2a_{11} + d_1a_{22})/2d_1d_2$ is the minimum value of k^2 for which $C(k^2)$ will attain its minimum value, say $C(k^2)_{min}$, such that

$$C(k^2)_{min} = (a_{11}a_{22} - a_{12}a_{21}) - \frac{(d_2a_{11} + d_1a_{22})^2}{4d_1d_2}$$

. This k_{min} is the critical wave number for Turing instability. And, the critical diffusion coefficient (Turing bifurcation threshold) $d_{1[c]}$ such that $C(k^2)_{min} = 0$ is given as

$$d_{1[c]} = \frac{d_2(a_{11}a_{22} - 2a_{12}a_{21}) - \sqrt{d_2^2(a_{11}a_{22} - 2a_{12}a_{21})^2 - d_2^2a_{11}^2a_{22}^2}}{a_{22}^2}. \quad (3.4)$$

The system will show stationary and non-stationary patterns for $d_1 < d_{1[c]}$, but the coexisting equilibrium (u^*, v^*) of the local model (2.5) remains stable under random heterogeneous perturbation when $d_1 > d_{1[c]}$.

Moreover, to ensure the positivity of $k^2 = k_{min}^2$ at the Turing bifurcation threshold, we need to have $d_2a_{11} + d_1a_{22} > 0$, i.e., $d_1 < d_2$ needs to be satisfied for the Turing instability conditions. Hence, the self-diffusion coefficient of the prey population is less than that of the predator population for the model (2.5).

The wavelength at the Turing bifurcation threshold is $\lambda_m = 2\pi/k_m$ where k_m is the wavenumber corresponding to the maximum real part of the positive eigenvalue. If the above necessary condition holds and $min_{k^2} < 0$ with certain k^2 in the interval of (ζ^-, ζ^+) where

$$\begin{aligned} \zeta^+(d_1) &= \frac{(d_2a_{11} + d_1a_{22}) + \sqrt{(d_2a_{11} + d_1a_{22})^2 - 4d_1d_2 \det(\mathbf{J}(E^*))}}{2d_1d_2} \\ \zeta^-(d_1) &= \frac{(d_2a_{11} + d_1a_{22}) - \sqrt{(d_2a_{11} + d_1a_{22})^2 - 4d_1d_2 \det(\mathbf{J}(E^*))}}{2d_1d_2}. \end{aligned} \quad (3.5)$$

Then (u^*, v^*) is an unstable homogeneous steady-state of system (2.5). Summarizing the conditions, we get the following theorem:

Theorem 3.5. *Considering that the interior equilibrium point (u^*, v^*) is locally asymptotically stable, if the following conditions hold*

$$(d_2a_{11} + d_1a_{22})^2 > 4d_1d_2 \det(\mathbf{J}(E^*)), \quad d_1 < d_2 \quad (3.6)$$

and there exists a wave-number $k^2 \in (\zeta^-, \zeta^+)$, then the positive constant steady-state solution (u^, v^*) of model (2.5) is Turing unstable.*

The Turing instability analysis for the proposed nonlocal model is almost similar to the analysis corresponding to the spatio-temporal (local) model (2.5). The inclusion of nonlocal range δ will lead to some differences in the Turing domain, and it is described in Appendix B.

4. Numerical Results

This section has validated the proven analytical findings through numerical simulation. First, the dynamics of the temporal model are explored, and then the significance of incorporating the spatio-temporal model is analyzed. Later, we demonstrated how nonlocal interaction has influenced the dynamic nature of the system. Unless it is mentioned otherwise, we fix some of the parameters used in the model, which are given in Table 1.

Parameter	r	ω	a	m	b	α	η	A	d	p	c	l	μ_1	μ_2
Value	1	10	0.36	0.42	0.5	0.5	0.05	2	0.05	0.05	0.9	0.005	0.1	0.05

Table 1: Parameter values used in the numerical simulations

4.1. Temporal dynamics

As we have emphasized the impact of the psychological effect on predator-prey interaction in this work, the fear effect can be considered one of the prime factors in analyzing the system dynamics. Moreover, we have already mentioned that the predators affect each other's activity while hunting and searching for prey. So, a predator-dependent functional response is the most suitable one, and it is considered in this work.

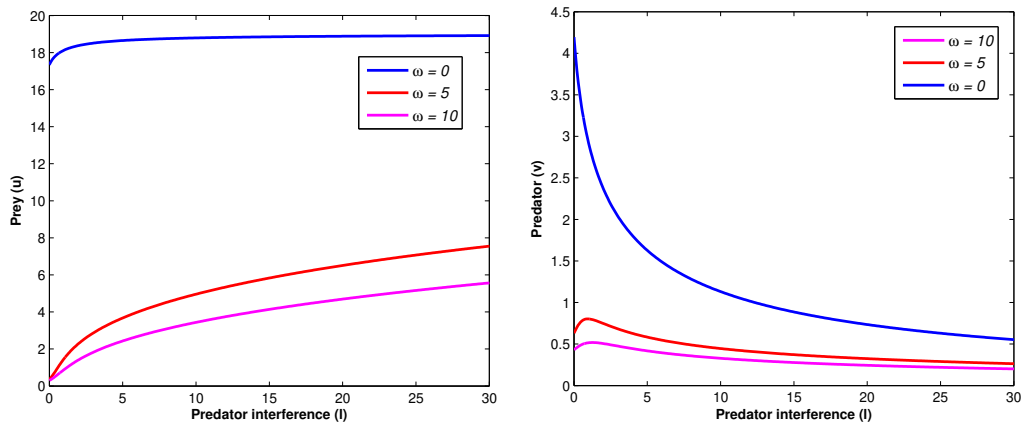


Figure 1: Impact of predator interference on (a) prey (u) and (b) predator (v) population in the presence and absence of the fear effect.

Figure 1 depicts how the fear effect reduces the population count in the presence of predator interference (l). It is observed that the more they intrude on each other's business, the more the prey count increases. And this predator interference is more effective when a certain amount of fear exists in the system. Furthermore, the counts of prey (u) and predator (v) species are shown in Fig. 2 for increasing the value of fear level (ω). In this case, the prey species has shown a declination for increasing value of ω , which causes the reduction in predator population too. But, in this work, we have dealt with the fear effect and provided a source of alternative or additional food to the predators. This figure supports the fact that the inclusion of alternative food helps to increase the prey population as they get a chance to save themselves by hiding in

a safe zone, creating prey refuge while predators are busy with secondary food sources, further increasing the predator count.

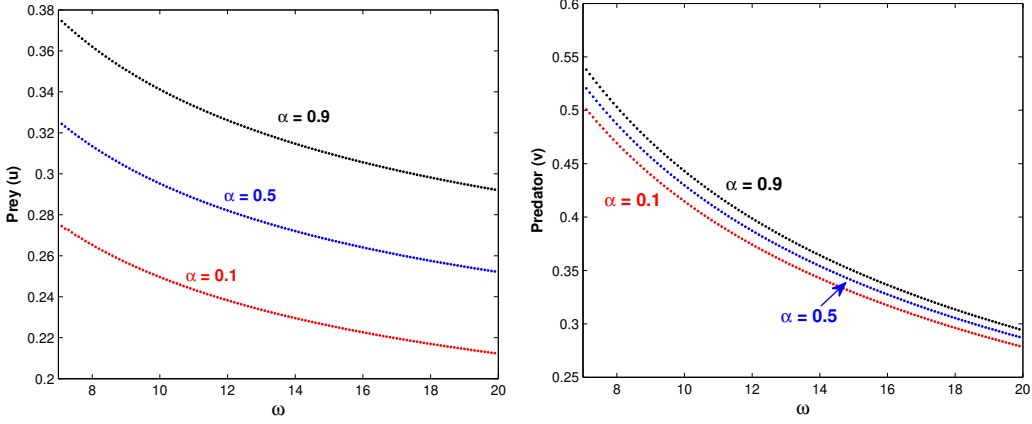


Figure 2: Comparison of the components of E^* for $\alpha = 0.1, 0.5, 0.9$ while varying ω .

We portray some scenarios in Fig. 3 when different system parameters are chosen as control parameters. First, it is observed that the consumption rate of predator (a) contributes to the existence of the steady coexisting state [see Fig. 3(a)]. If the predator consumes the targeted prey at a very low rate to their growth, then they may not be able to survive in the system even if there is some additional food present, and a stable predator-free system occurs in such cases (e.g., stable E_1 in our case). But from this situation, if the consumption rate starts to increase, then a situation arises where both prey and predator exist in a steady state (e.g., stable coexisting equilibrium E^*). In this case, the coexisting equilibrium point switches the stability behaviour from the predator-free equilibrium E_1 through transcritical bifurcation. For the considered parameter set, this transcritical bifurcation occurs at $a = a_{[TC_1]} = 0.115608$ [see Fig. 3(a)]. A further increment of the parameter a leads to the extinction of prey species, and only predator species exist in a steady state in such cases (e.g., stable prey-free equilibrium E_2). In this case, the coexisting equilibrium point and prey-free equilibrium point exchange their stabilities through another transcritical bifurcation that occurs at $a = a_{[TC_2]} = 0.699983$ [see Fig. 3(a)].

We have studied the model's behaviour when the predators go for additional food sources instead of the targeted prey, and the parameter η is involved in signifying it. Figure 3(b) shows that if the predator detects the additional food up to a certain amount along with the prey species, then both the population exist as a steady state, but increasing the parametric value leads to a situation where the two equilibrium points E_2 and E^* exchange their stability through a transcritical bifurcation which occurs at $\eta = \eta_{[TC_1]} = 0.115306$. The prey-free equilibrium exists for $\eta > \eta_{[TC_1]}$. Also, there exists an unstable branch of E_2 when η lies below $\eta_{[TC_1]}$, which ultimately emerges with the unstable trivial equilibrium E_0 through another transcritical bifurcation at $\eta = \eta_{[TC_2]} = 0.091241$.

Now, we see how the intra-specific mortality rate of predators regulates the system dynamics, which can be controlled by the parameter μ_2 . When a predator is exposed to prey species that are inadequate in the system, they tend to compete with each other to gain more food. This psychology remains the same even in the presence of alternative food sources. Figure 3(c) shows that a certain amount of competition is needed for the coexisting equilibrium point. But both the populations start to oscillate around E^* if μ_2 comes below a certain threshold value through Hopf bifurcation, which occurs at $\mu_{2[H]} = 0.032103$. In this case, the temporal model exhibits a

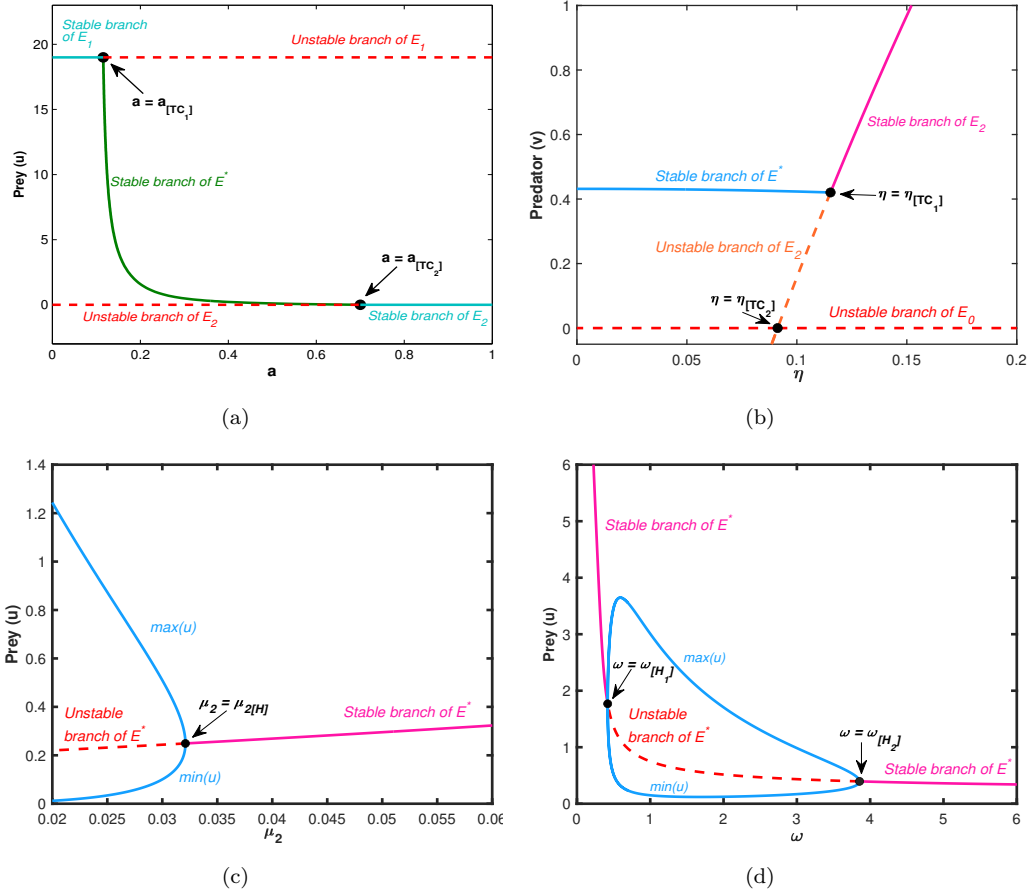


Figure 3: Change of dynamical behaviour of temporal system (2.4) with increasing (a) c , (b) η , (c) μ_2 and (d) ω .

supercritical Hopf bifurcation, and the first Lyapunov coefficient is $l_1 = -0.0294$. Furthermore, it is observed that the fear term (ω) acts as a stabilizing as well as destabilizing factor in the system [see Fig. 3(d)]. Both the populations coexist and are stable for a small value of ω , but an increase in the value leads to oscillation, indicating the occurrence of a supercritical Hopf bifurcation at $\omega_{[H_1]} = 0.419521$ with the first Lyapunov coefficient $l_1 = -0.0162$. A stable limit cycle is generated through this Hopf bifurcation and vanishes through another supercritical Hopf bifurcation at $\omega_{[H_2]} = 3.855245$ with $l_1 = -0.0305$. With further increased fear parameter value ω , the coexisting equilibrium point remains stable [see Fig. 3(d)].

Sometimes, a predator fails to access the whole of the prey population when a prey species successfully hides in a safe zone to dodge the frequent attack of their predator. The prey refuge parameter (m) in the model can capture this scenario. Figure 4(a) shows that the coexisting equilibrium point can be obtained when a certain amount of prey hides in a predator-prohibited zone, but both populations perform oscillatory behaviour if the prey refuge parameter comes below a threshold value. This situation occurs in the system through a supercritical Hopf bifurcation around the coexisting equilibrium point E^* at $m_{[H]} = 0.302811$ (the first Lyapunov coefficient is $l_1 = -0.0389$), and stable limit cycle exists for $m < m_{[H]}$. Furthermore, the predator count has been plotted by taking the prey refuge parameter (m) in Fig. 4(b) in the absence and presence of additional food sources. It is seen that the Hopf threshold shifts towards the left due to the incorporation of additional food. Therefore, the additional food expands the region where the population can coexist as the population oscillates whenever m is less than the Hopf threshold [see Fig. 4(a)].

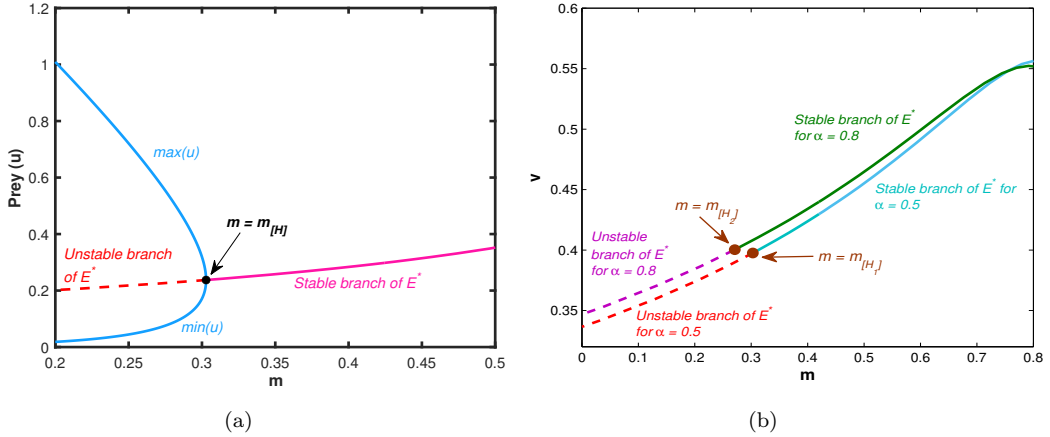


Figure 4: (a) Change of dynamical behaviour of the temporal system with increasing m . (b) Impact of prey refuge (m) on the predator population (v) in the presence of alternative food sources.

4.2. Effects of local and nonlocal interactions

We first analyze the results by incorporating local interactions in the temporal model. This work focuses on studying the impact of fear in the presence of additional food sources. So, we choose the additional food source ω as the bifurcation parameter. Turing instability is one of the main factors studied in the reaction-diffusion model, which helps to find non-homogeneous stationary patterns. For finding such Turing instability, the coexisting homogeneous steady-state has to be locally asymptotically stable. In our temporal model, there exists two Hopf bifurcation thresholds $\omega_{[H_1]}$ and $\omega_{[H_2]}$. The stable coexisting equilibrium point is found when ω lies outside these thresholds, and the system shows periodic dynamics inside these thresholds [see Fig. 3(d)]. We first focus on the temporal Hopf stable domain $\omega > \omega_{[H_2]}$.

For a fixed ω , we obtain the Turing bifurcation threshold $d_{1[c]}$, and we plot this set of Turing bifurcation thresholds for a set of parameter values of ω in the ω - d_1 plane, which is shown in Figure 5. We have plotted the Turing curve and temporal Hopf curve here, which intersect each other, and they divided the region into four sub-regions. Pure Turing domain (R_1) and homogeneous solution (R_4) lie on the right of the second Hopf curve $\omega = \omega_{[H_2]}$, below and above the Turing curve, respectively. On the other hand, there is another Turing domain (R_5) and homogeneous solution (R_6) exist left to the first Hopf curve $\omega = \omega_{[H_1]}$, below and above Turing curve respectively. The bottom region (R_2) between the two temporal Hopf curves is the Turing-Hopf domain, while the upper region (R_3) is the Hopf domain. Here, we have mainly chosen the values of ω and d_1 from R_1, R_2, R_3 and R_4 domains as the other two regions R_5 and R_6 will show the same dynamical nature as R_1 and R_4 respectively.

To describe the Turing and non-Turing patterns for the system (2.5), we have chosen the spatial domain as $[-L, L]$, where $L = 50$, with non-negative initial and periodic boundary conditions. A heterogeneous perturbation is given around the coexisting homogeneous steady-state as the initial conditions to observe the dynamics. We choose small amplitude random perturbations given by $u(x_j, 0) = u^* + \epsilon \xi_j$ and $v(x_j, 0) = v^* + \epsilon \psi_j$ with $\epsilon = 10^{-5}$ and ξ_j and ψ_j are Gaussian white noise δ -correlated in space. The dynamical behaviour of the proposed spatio-temporal model is explored in Figs. 5–9. It is also noted that the nonlocal model (2.6) turns into a local model (2.5) if the range of nonlocal interaction δ tends to 0.

For $\omega = 10$ the temporal model (2.5) has the feasible interior equilibrium point $E^* = (0.295, 0.430)$, which is stable. Also, from equation (3.4), $d_{1[c]}$ is found to be 0.0406 when $d_2 = 10$. The real part of an eigenvalue is plotted in Fig. 6 when d_1 is chosen from Turing domain (R_1) [see Fig. 6(a)], Turing-Hopf domain (R_2) [see Fig. 6(b)] and Hopf domain (R_3)

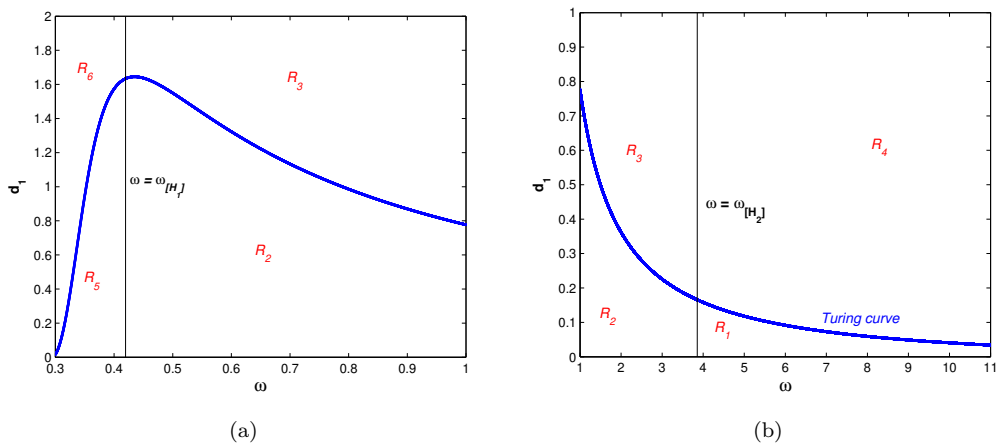


Figure 5: Temporal-Hopf, Turing bifurcation curves in the ω - d_1 plane for the local model are represented by black and blue colors. The Turing domain corresponding to (a) $\omega < \omega_{[H_1]}$ and (b) $\omega > \omega_{[H_2]}$ is considered here.

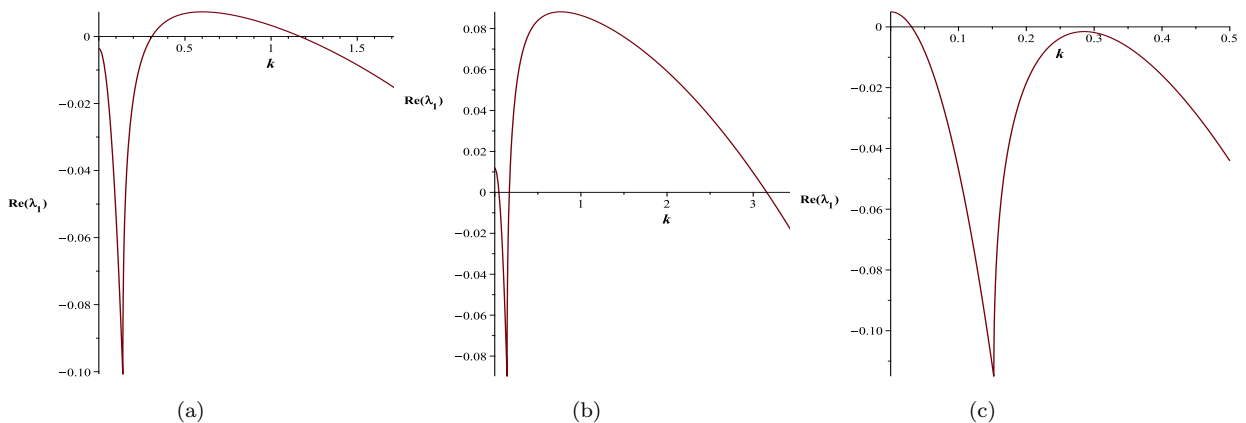


Figure 6: Plot of largest real part of eigenvalues with respect to k when (ω, d_1) are chosen from R_1, R_2 and R_3 respectively. (a) Turing domain: $(\omega, d_1) = (10, 0.01)$, (b) Turing-Hopf domain: $(\omega, d_1) = (1, 0.01)$ and (c) Hopf domain: $(\omega, d_1) = (2, 0.38)$

[see Fig. 6(c)]. Here, the real parts match the cases for the temporal model for $k = 0$. The oscillatory solution also occurs for the local model in the domain above the Turing curve and to the left of the temporal Hopf curve. These oscillatory solutions are homogeneous in space but periodic in time. A sample solution is plotted in Fig. 7 for $\omega = 2$ and $d_1 = 0.38$.

Some literature already states that if a specialist predator is considered in a predator-prey model, then time-dependent spatial patterns occur when the diffusion parameter is chosen from a bit inside of the temporal Hopf domain [49, 50]. The Turing behaviour mainly dominates and creates stationary patterns in the Turing-Hopf domain. However, the Hopf behaviour also dominates and produces oscillatory patterns. These oscillatory solutions can be found in this domain in a small region near the Turing curve. Generally, non-homogeneous stationary patterns exist in most parts of the Turing-Hopf domain for the local model, depicted in Figs. 8 for $d_1 = 0.01$ and with $\omega = 1$.

When $d_1 > d_{1[c]}$ holds in the right of the temporal Hopf curve, the stationary homogeneous solution can be obtained in the stable domain (R_4). However, a decrease of the diffusion parameter d_1 makes a shift in the Turing domain (R_1), where Turing pattern solutions can be obtained for the mentioned boundary condition. In order to draw Fig. 9, let us choose $d_1 = 0.01$ from the Turing domain (see R_1 in Figure 5) when $\omega = 10$. The figure depicts the stationary Turing patterns for the periodic boundary condition when parameter values are chosen from

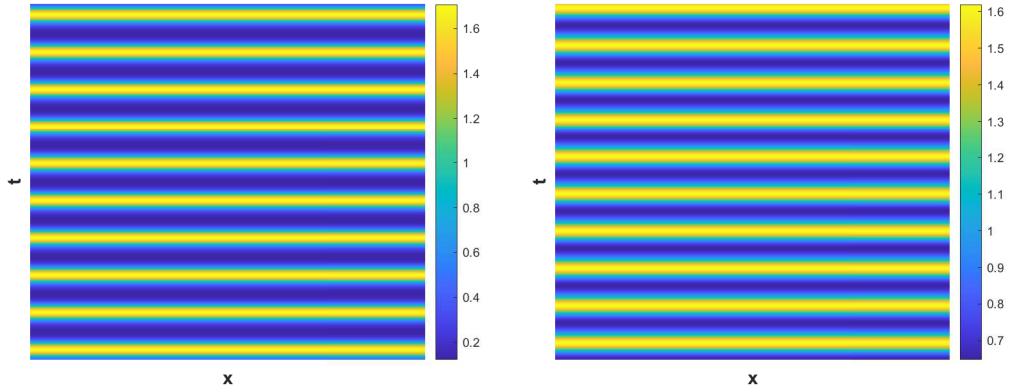


Figure 7: Contour plot of u (left) and v (right) of the local model for $\omega = 2$ when $d_1 = 0.38$ is chosen from Hopf domain (R_3).

Table 1 along with $d_2 = 10$. The figure shows that the amplitude of the pattern is constant in the whole domain.

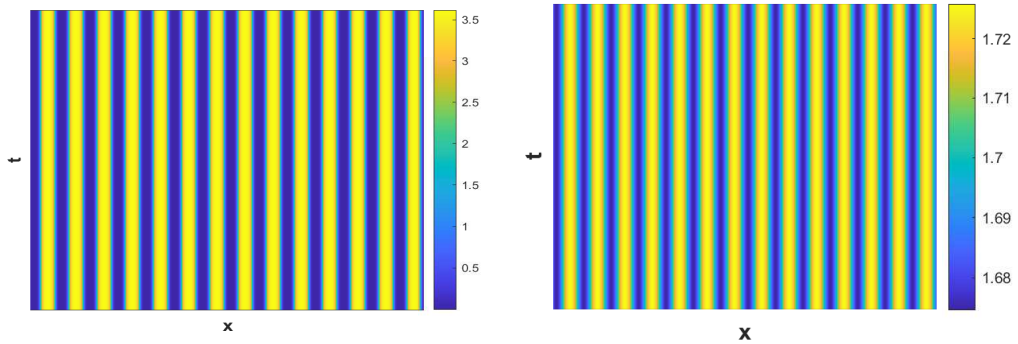


Figure 8: Contour plot of u (left) and v (right) of system (2.5) for $\omega = 1$ when $d_1 (= 0.01)$ is chosen from Turing-Hopf domain (R_2).

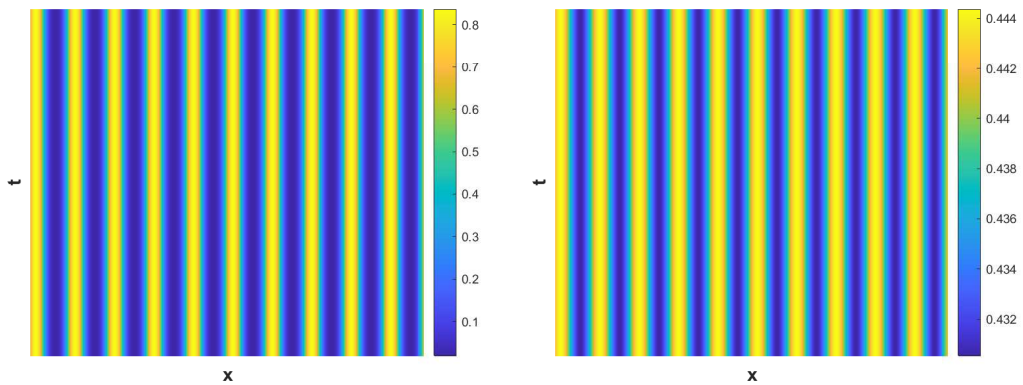


Figure 9: Contour plot of u (left) and v (right) of system (2.5) for $\omega = 10$ when $d_1 (= 0.01)$ is chosen from Turing domain (R_1).

Now, we study the behaviour of the nonlocal model (2.6) for different values of the range of nonlocal interactions δ . The temporal Hopf bifurcation curve is independent of δ . However, the Turing bifurcation curve depends on δ . We have plotted the Turing bifurcation curves in

Fig. 10 for different values of the range of nonlocal interaction. This figure shows that the Turing curve shifts upwards with an increase in the interaction range δ . This figure shows the difference between the Turing curves for local and nonlocal models to emphasize the significance of nonlocal terms in the system. Furthermore, it indicates that including nonlocal interaction expands the Turing domain by increasing the chance of occurrence of stationary patterns in the population.

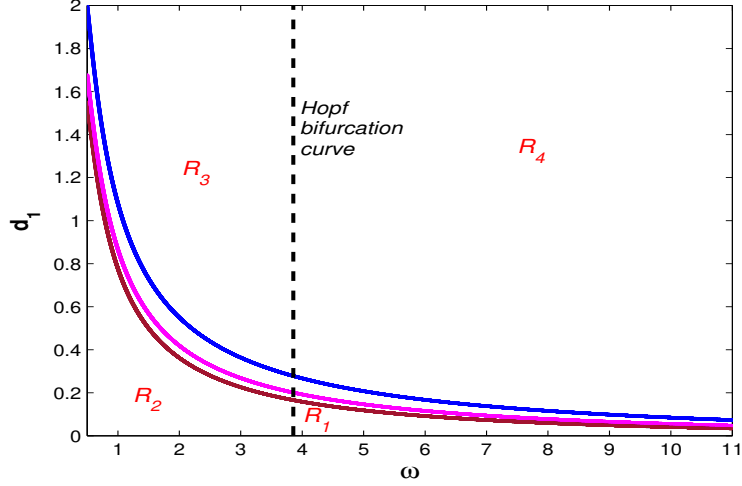


Figure 10: Temporal-Hopf curve and Turing curves for local and nonlocal models. The temporal-Hopf curve is represented by black color. The maroon color curve denotes the Turing curve for the local model, and the magenta and blue color curves are the Turing curve for $\delta = 5$ and $\delta = 10$, respectively.

Now, we find the solution characteristics for the nonlocal model in each domain formed due to the intersection of the temporal Hopf and Turing curves. For a certain nonlocal interaction δ , first, we consider the region to the right of the temporal Hopf curve. The pure Turing domain is the region that lies below the Turing curve. On the other hand, the stable region lies above the Turing curve, where the solutions are homogeneous under the heterogeneous perturbations around the coexisting steady state. The region above the Turing curve and to the left of the temporal Hopf curve is called the Hopf domain. Finally, the region lying to the left of the temporal-Hopf curve and below the Turing curve is called the Turing-Hopf domain.

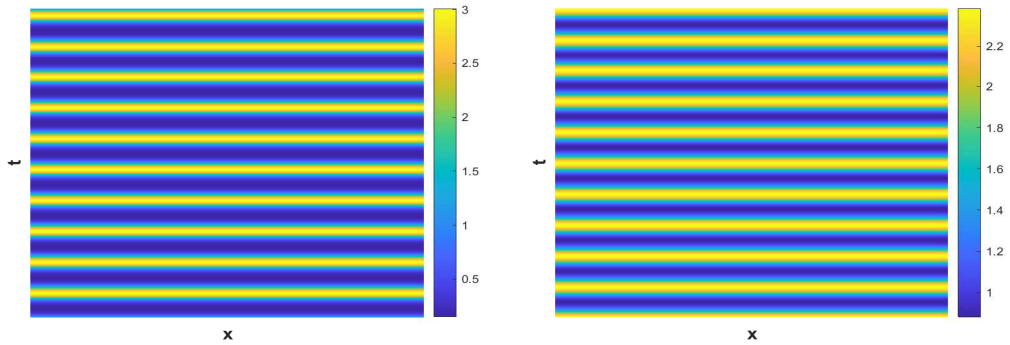


Figure 11: Contour plot of u (left) and v (right) of the nonlocal model for $\omega = 2$ when $d_1 (= 2.5)$ is chosen from Hopf domain (R_3).

Let us first explore the solutions of the nonlocal model in the temporal Hopf unstable domain. We have chosen $\omega = 2$ and $\delta = 10$ and plot the corresponding solutions of the

nonlocal model for $d_1 = 2.5$ and $d_1 = 0.38$ in Figs. 11 and 12, respectively. The value $d_1 = 2.5$ lies above the Turing curve, and the other values $d_1 = 0.45$ and $d_1 = 0.38$ lie in the Turing-Hopf domain away and near the Turing curve. We mainly intend to observe if the dynamical nature changes in the presence of nonlocal interaction. The oscillatory solution occurs for system (2.6) in the Hopf domain, which is homogeneous in space but periodic in time [see Fig. 11 for $\omega = 2$ and $d_1 = 2.5$]. In the Turing-Hopf domain, the dominance of Hopf mode can be seen for the nonlocal model when the parameter values lie close to the Turing curve. Moreover, a decrease in the value of d_1 ultimately gives non-homogeneous stationary patterns for the nonlocal model, which is reflected in Figure 12.

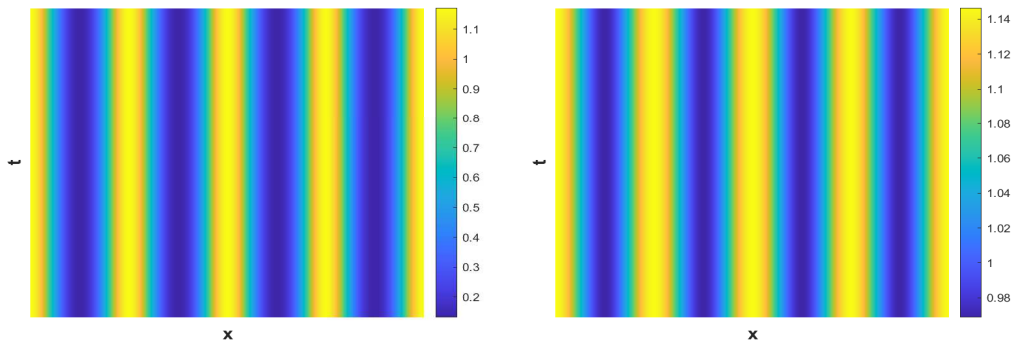


Figure 12: Contour plot of u (left) and v (right) of system (2.6) for $\omega = 2$ when $d_1 (= 0.38)$ is chosen from Turing-Hopf domain (R_2).

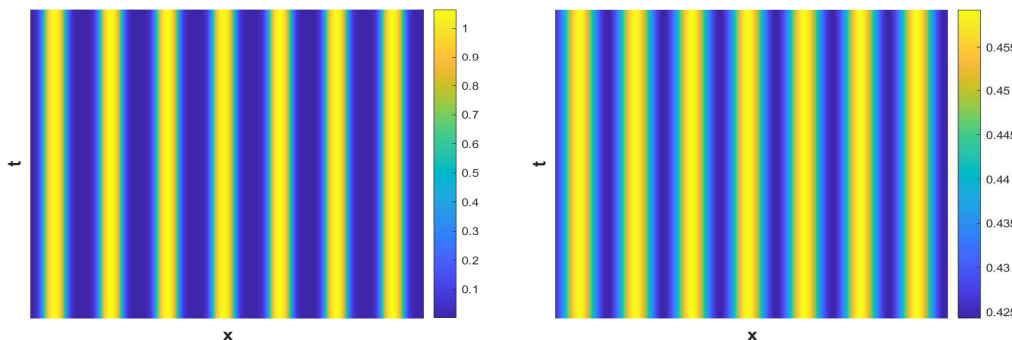


Figure 13: Contour plot of u (left) and v (right) of system (2.6) for $\omega = 10$ when $d_1 (= 0.01)$ is chosen from Turing domain (R_1).

For the nonlocal model, it is observed that if $d_1 < d_{1[c]}^T$ holds in the right of the temporal Hopf curve, then it produces stationary Turing patterns. For instance, a Turing pattern is shown in Fig. 13 for $d_1 = 0.01$ and $\omega = 10$. In addition, we have compared the behaviours of local and nonlocal models for the parameters that lie in the temporal Hopf unstable domain. We choose the parameter values as $\omega = 2$ and $d_1 = 0.38$ for this. In this case, the local model shows periodic dynamics in time and homogeneous in space [see Fig. 7], but the nonlocal model shows the non-homogeneous stationary solution for $\delta = 10$ [see Fig. 12]; these two types of dynamics happen due to the shifting of the Turing curve. The parameter d_1 lies in the Hopf unstable domain for the local model; however, it lies in the Turing-Hopf domain for the nonlocal model with $\delta = 10$, and the Turing structure dominates the oscillation behaviour in this case. This further shows that the nonlocal interaction enhances the region's ability to get non-homogeneous stationary patterns, which is beneficial for their survival in the long run.

5. Conclusions

In an ecological system, predator-prey interaction is a biological phenomenon that balances the food web. The sustainability of predatory species depends on their consumption process and search strategy for prey. This consumption process by predators depends on resource population size, availability, and the interference of other predators. Sometimes, the growth of prey becomes affected by the frequent attacks of their predator. Research reveals that only the fear of predation reduces the reproduction of song sparrows [2, 10]. Also, the fear of being consumed by large carnivores leads to a decline in mesocarnivores' foraging time and strategy [8]. There are already some works published where the involvement of fear of predation is analysed in predator-prey interactions, but the nonlocal interaction is not considered there. In the current work, we have explored how incorporating nonlocal terms influences population colonization.

Here, we have proposed a predator-prey interaction that includes psychological stress in the prey species induced by the fear of their predators. The main intention here is to elucidate the importance of this factor in the dynamic behaviour of the model, as we have assumed that the growth rate of prey is reduced due to fear of predation. Along with the fear term, we have considered the interference of predators while searching or handling their prey by choosing the Beddington-DeAngelis functional response. And, as we have assumed that the predator is provided with alternative food sources, it is evident that the prey will get the scope to move towards a predator-prohibited zone by creating prey refuge, which leaves only a fraction of them for the predators for consumption. In this work, we have explored how all these factors impact the dynamics of these species' interactions. It is observed in the numerical simulation that the consumption rate of predators plays an important role as the system can move to a steady prey-free state or even predator-free state from a stable coexistence state while regulating this parameter [see Fig. 3(a)]. In fact, the detection of additional food (η) also has the ability to regulate the dynamics as we have found stable interior equilibrium (E^*) from predator-free state (E_2) by decreasing its value. As the prey species creates some refugia while the predator engages with additional food, the prey species can save themselves from going extinct, and steady coexistence occurs among populations [see Fig. 3(b)]. The prey refuge (m) also has the regulation ability as Fig. 4 shows that when the refuge parameter lies below a threshold value, the population oscillates, but we get coexistence while m exceeds the Hopf threshold. Not only that, but the presence of additional food increases the chances of such coexistence. Now, the fear level has been found to be a stabilizing as well as destabilizing factor in this model [see Fig. 3(d)]. Though a stable coexisting state found for a very small as well as large value of fear ($\omega < \omega_{[H_1]}$ and $\omega > \omega_{[H_2]}$), but oscillation is observed when it lies within a range $\omega \in (\omega_{[H_1]}, \omega_{[H_2]})$. It indicates that a certain amount of fear is needed in the system for the population to coexist.

In the later part of the work, it is assumed that the species can move in one direction described by the spatio-temporal model. The analysis reveals that the diffusion coefficient for the prey species starts to decrease with increasing fear level (ω) [see Fig. 5]. It indicates that the prey, out of fear of being hunted, will avoid moving in the mentioned direction. In fact, the increase in ω shrinks the region of the Turing domain, reducing the chances of non-homogeneous pattern formation. As the species are not always homogeneously distributed over a domain, this shrinkage may not be favourable for persistence. Further, incorporating nonlocal terms in the system shifts the Turing curve upwards, expanding the Turing domain. This means that the species can be colonized with an increasing range of nonlocal interactions, which will benefit both species' survival in the future.

Though the proposed system contains rich dynamics, it can be refined further. It is as-

sumed that the growth of prey species is affected by fear of the predator, which is one of the constraints under which the system is formulated. However, the prey species may adopt different defence mechanisms as a counteraction in the natural environment. Therefore, considering the contribution of group defence in the prey's growth will move the situation closer to reality. Moreover, in ecological systems, the carryover effect may occur in any predator-prey interaction where species' past experiences and background are used to explain their present behaviour. The fear of predation is considered one of the non-lethal effects of the predator on prey, which may not affect a single generation only but can be carried over to the next generations. So, this carryover effect can be incorporated into the prey species of the model (2.4). Furthermore, the environmental stochasticity remains uncultivated in this work, which can be proposed in the system through white Gaussian noise. In the proposed model, we have considered that only a fixed portion of prey hide successfully, but in the future, this model can be refined by introducing a predator-dependent refuge function. So, the system (2.4) will become even more realistic when these aspects are incorporated and analyzed.

5.1. Acknowledgements

The authors are grateful to the NSERC and the CRC Program for their support. RM is also acknowledging the support of the BERC 2022–2025 program and the Spanish Ministry of Science, Innovation and Universities through the Agencia Estatal de Investigacion (AEI) BCAM Severo Ochoa excellence accreditation SEV-2017–0718. This research was enabled in part by support provided by SHARCNET (www.sharcnet.ca) and Digital Research Alliance of Canada (www.alliancecan.ca).

5.2. Data Availability Statement

The data used to support the findings of the study are available within the article.

5.3. Conflict of Interest

This work does not have any conflict of interest.

Appendix A

A.1 Proof of positivity and boundedness of variables of model (2.4)

Functions on the right-hand side of the system (2.4) are continuous and locally Lipschitzian (as they are polynomials and rationals in (u, v)), so there exists a unique solution $(u(t), v(t))$ of the system with positive initial conditions $(u(0), v(0)) > 0$ on $[0, \tau]$, where $0 < \tau < +\infty$ [51]. From the first, and second equation of (2.4) we have

$$\begin{aligned} \frac{du}{dt} &= u \left[\frac{r}{1 + \omega v} - d - pu - \frac{a(1 - m)v}{b + \alpha\eta A + (1 - m)u + lv} \right] = u\psi_1(u, v) \\ \Rightarrow u(t) &= u(0) \exp \left[\int_0^t \psi_1(u(z), v(z)) dz \right] > 0, \text{ for } u(0) > 0. \end{aligned}$$

$$\begin{aligned} \text{And, } \frac{dv}{dt} &= v \left[\frac{ca\{(1 - m)u + \eta A\}}{b + \alpha\eta A + (1 - m)u + lv} - \mu_1 - \mu_2 v \right] = v\psi_2(u, v) \\ \Rightarrow v(t) &= v(0) \exp \left[\int_0^t \psi_2(u(z), v(z)) dz \right] > 0, \text{ for } v(0) > 0. \end{aligned}$$

So, the solutions of the system (2.4) are feasible with time.

Now, the first equation of (2.4) gives:

$$\begin{aligned}\frac{du}{dt} &= \frac{ru}{1+\omega v} - du - pu^2 - \frac{a(1-m)uv}{b+\alpha\eta A+(1-m)u+lv} \leq (r-d)u \left[1 - \frac{pu}{r-d}\right] \\ \Rightarrow \limsup_{t \rightarrow \infty} u(t) &\leq \frac{r-d}{p}\end{aligned}$$

Consider, $W(t) = u(t) + \frac{1}{c}v(t)$. Then for any $\eta > 0$ we have

$$\begin{aligned}\text{So, } \frac{dW}{dt} + \eta W &= \left(\frac{du}{dt} + \frac{1}{c}\frac{dv}{dt}\right) + \eta u + \frac{\eta}{c}v \\ &\leq u[(r-d) - pu + \eta] + \frac{a\eta Av}{b+\alpha\eta A+(1-m)u+lv} - \frac{\mu_1}{c}v + \frac{\eta}{c}v \\ &\leq \frac{(r-d+\eta)^2}{4p} + \frac{a\eta A}{l} - \frac{v}{c}(\mu_1 - \eta)\end{aligned}$$

Choosing sufficiently small $\eta \ll \mu_1$, we obtain

$$\frac{dW}{dt} + \eta W \leq \left[\frac{(r-d+\eta)^2}{4p} + \frac{a\eta A}{l}\right] = M$$

By applying Gronwall's inequality, we have then $0 \leq W(t) \leq \frac{M}{\eta}(1 - \exp(-\eta t)) + W(u(0), v(0)) \exp(-\eta t)$.

As $t \rightarrow \infty$, $0 < W(t) \leq M/\eta + \epsilon$ for sufficiently small $\epsilon > 0$. So, the solutions of system (2.4) enter into the bounded region:

$$\Omega = \{(u, v) : 0 \leq u(t) \leq (r-d)/p; 0 \leq W(t) \leq M/\eta + \epsilon, \epsilon > 0\}.$$

A.2 Proofs of local stability conditions of the equilibrium points of system (2.4)

The Jacobian matrix corresponds to $E_0(0, 0)$ is given as

$$\mathbf{J}|_{E_0} = \begin{pmatrix} r-d & 0 \\ 0 & \frac{c\alpha\eta A}{s} - \mu_1 \end{pmatrix}$$

which gives $\lambda_1 = r-d$ and $\lambda_2 = c\alpha\eta A/s - \mu_1$. It means $\lambda_2 < 0$ when $c\alpha\eta A < \mu_1 s$ but $\lambda_1 > 0$ always (as the system is bounded). As one of the eigenvalues is positive, and hence, E_0 is an unstable equilibrium point.

Moreover, the Jacobian matrix at $E_1(\bar{u}, 0)$ is

$$\mathbf{J}|_{E_1} = \begin{pmatrix} b_{11} & b_{12} \\ 0 & b_{22} \end{pmatrix} = \begin{pmatrix} -p\bar{u} & -r\omega\bar{u} - \frac{a(1-m)\bar{u}}{s+(1-m)\bar{u}} \\ 0 & \frac{ca\{(1-m)\bar{u}+\eta A\}}{s+(1-m)\bar{u}} - \mu_1 \end{pmatrix},$$

The eigenvalues are the roots of the equation: $\lambda^2 + C_1\lambda + C_2 = 0$, where $C_1 = -(b_{11} + b_{22})$ and $C_2 = b_{11}b_{22}$. So, the equation has roots with negative real parts if $C_1 > 0$ and $C_2 > 0$ and this occurs when $b_{22} < 0$, i.e., $(ca - \mu_1)(1-m)\bar{u} < \mu_1 s - c\alpha\eta A$.

Again, the Jacobian matrix corresponds to $E_2(0, \tilde{v})$ is denoted as

$$\mathbf{J}|_{E_2} = \begin{pmatrix} b_{11} & 0 \\ b_{21} & b_{22} \end{pmatrix} = \begin{pmatrix} \frac{r}{1+\omega\tilde{v}} - \frac{a(1-m)\tilde{v}}{s+l\tilde{v}} - d & 0 \\ \frac{ca(1-m)\tilde{v}\{b+l\tilde{v}+\eta A(\alpha-1)\}}{(s+l\tilde{v})^2} & -\mu_2\tilde{v} - \frac{c\alpha\eta A\tilde{v}}{(s+l\tilde{v})^2} \end{pmatrix},$$

The eigenvalues are the roots of the equation: $\lambda^2 + D_1\lambda + D_2 = 0$, where $D_1 = -(b_{11} + b_{22})$ and $D_2 = b_{11}b_{22}$. The equation has roots with negative real parts if $D_1 > 0$ and $D_2 > 0$ and this occurs when $b_{11} < 0$, i.e., $\omega\{dl + a(1-m)\}\tilde{v}^2 + \{dsw + a(1-m) - (r-d)l\}\tilde{v} - (r-d)s > 0$.

Lastly, the Jacobian matrix corresponds to $E^*(u^*, v^*)$ is given as

$$\mathbf{J}(E^*) = \mathbf{J}|_{E^*} = \begin{pmatrix} a_{11} & a_{12} \\ a_{21} & a_{22} \end{pmatrix},$$

$$\text{where } a_{11} = -pu^* + \frac{a(1-m)^2u^*v^*}{[s + (1-m)u^* + lv^*]^2}, \quad a_{12} = -r\omega u^* - \frac{a(1-m)u^*[s + (1-m)u^*]}{[s + (1-m)u^* + lv^*]^2},$$

$$a_{21} = \frac{ca(1-m)v^*[b + lv^* + \eta A(\alpha - 1)]}{[s + (1-m)u^* + lv^*]^2} \quad \text{and} \quad a_{22} = -\mu_2v^* - \frac{ca\{(1-m)u^* + \eta A\}lv^*}{[s + (1-m)u^* + lv^*]^2}.$$

The characteristic equation corresponding to $\mathbf{J}|_{E^*}$ is given as follows:

$$\lambda^2 + F_1\lambda + F_2 = 0, \quad (\text{A.1})$$

where $F_1 = -\text{tr}(\mathbf{J}(E^*)) = -(a_{11} + a_{22})$ and $F_2 = \det(\mathbf{J}(E^*)) = a_{11}a_{22} - a_{12}a_{21}$. So, by Routh-Hurwitz criteria, the equilibrium point will be locally asymptotically stable if the equation has roots with negative real parts, i.e., $F_1 > 0$ and $F_2 > 0$, i.e.,

$$a_{11} + a_{22} < 0 \quad \text{and} \quad a_{11}a_{22} > a_{12}a_{21}. \quad (\text{A.2})$$

So, the local asymptotic stability of E^* depends on the conditions: $av^*[(1-m)^2u^* - lc(1-m)u^* - lc\eta A] < (pu^* + \mu_2v^*)K^2$, and $p\mu_2K^4 + [ca\{pl\{(1-m)u^* + \eta A\} + r\omega(1-m)\{b + lv^* + \eta A(\alpha - 1)\}\} - a\mu_2(1-m)^2v^*]K^2 + ca^2(1-m)^2[\{s + (1-m)u^*\}\{b + lv^* + \eta A(\alpha - 1)\} + (s - \eta A)lv^*] > 0$, where $K = [s + (1-m)u^* + lv^*] > 0$.

A.3 Proofs of local bifurcations around the equilibrium points of system (2.4)

Let us consider $\mathbf{V} = (v_1, v_2)^T$ and $\mathbf{W} = (w_1, w_2)^T$, respectively be the eigenvectors of $\mathbf{J}|_{(eq. \text{ point})}$ and $\mathbf{J}|_{(eq. \text{ point})}^T$ for a zero eigenvalue at the equilibrium point. Let $\bar{\mathbf{F}} = (\bar{F}_1, \bar{F}_2)^T$, where

$$\bar{F}_1 = \frac{ru}{1 + \omega v} - du - pu^2 - \frac{a(1-m)uv}{b + \alpha\eta A + (1-m)u + lv},$$

$$\bar{F}_2 = \frac{ca\{(1-m)u + \eta A\}v}{b + \alpha\eta A + (1-m)u + lv} - \mu_1v - \mu_2v^2.$$

Now, the Jacobian matrix at E_1 is given by

$$\mathbf{J}|_{E_1} = \begin{pmatrix} b_{11} & b_{12} \\ 0 & b_{22} \end{pmatrix} = \begin{pmatrix} -p\bar{u} & -r\omega\bar{u} - \frac{a(1-m)\bar{u}}{s+(1-m)\bar{u}} \\ 0 & \frac{ca\{(1-m)\bar{u} + \eta A\}}{s+(1-m)\bar{u}} - \mu_1 \end{pmatrix},$$

The eigenvalues are the roots of the equation $\lambda^2 - (b_{11} + b_{22})\lambda + b_{11}b_{22} = 0$, which gives the roots with negative real parts. Let $a_{[TC_1]}$ be the value of a such that $(ca - \mu_1)(1-m)\bar{u} = \mu_1s - ca\eta A$ so that $\mathbf{J}|_{E_1}$ has a simple zero eigenvalue at $a_{[TC_1]}$. So, at $a = a_{[TC_1]}$:

$$\mathbf{J}|_{E_1} = \begin{pmatrix} b_{11} & b_{12} \\ 0 & 0 \end{pmatrix}.$$

The calculations give $\mathbf{V} = (v_1, v_2)^T$ where $v_1 = -b_{12}$, $v_2 = b_{11}$ and $\mathbf{W} = (0, 1)^T$. Therefore,

$$\begin{aligned}\Omega_1 &= \mathbf{W}^T \cdot \bar{\mathbf{F}}_a(E_1, a_{[TC_1]}) = \frac{c\{(1-m)\bar{u} + \eta A\}v}{\{s + (1-m)u + lv\}} \Big|_{E_1} = 0, \\ \Omega_2 &= \mathbf{W}^T [D\bar{\mathbf{F}}_a(E_1, a_{[TC_1]})\mathbf{V}] = \frac{c\{(1-m)\bar{u} + \eta A\}b_{11}}{\{s + (1-m)\bar{u}\}} \Big|_{E_1} \neq 0 \\ \text{and } \Omega_3 &= \mathbf{W}^T [D^2\bar{\mathbf{F}}(E_1, a_{[TC_1]})(\mathbf{V}, \mathbf{V})] \\ &= \frac{-2ca(1-m)\{b + \eta A(\alpha - 1)\}b_{11}b_{22}}{\{s + (1-m)\bar{u}\}^2} - 2 \left\{ \mu_2 + \frac{cal\{(1-m)\bar{u} + \eta A\}}{\{s + (1-m)\bar{u}\}^2} \right\} b_{11}^2 \neq 0.\end{aligned}$$

Then, by Sotomayor's Theorem, the system undergoes a transcritical bifurcation around E_1 at $a = a_{[TC_1]}$.

Similarly, we can prove that the system exhibits another transcritical bifurcation around E_2 at $a = a_{[TC_2]}$, where $a_{[TC_2]}$ is the positive root of the equation $\omega\{dl + a(1-m)\}\tilde{v}^2 + \{ds\omega + a(1-m) - (r-d)l\}\tilde{v} - (r-d)s = 0$.

Now, for the existence of Hopf bifurcation around E^* , at $\omega = \omega_{[H]}$, the characteristic equation of system (2.4) at E^* is $(\lambda^2 + F_2) = 0$ and so, the equation has a pair of purely imaginary roots $\lambda_1 = i\sqrt{F_2}$ and $\lambda_2 = -i\sqrt{F_2}$ where $F_2(\omega)$ is a continuous function of ω .

In the small neighbourhood of $\omega_{[H]}$, the roots are $\lambda_1 = p_1(\omega) + ip_2(\omega)$ and $\lambda_2 = p_1(\omega) - ip_2(\omega)$ ($p_1, p_2 \in \mathbb{R}$).

To show the transversality condition, we need to check $\left(\frac{d}{d\omega} [Re(\lambda_i(\omega))] \right) \Big|_{\omega=\omega_{[H]}} \neq 0$, for $i = 1, 2$.

Put $\lambda(\omega) = p_1(\omega) + ip_2(\omega)$ in (A.1), we get

$$(p_1 + ip_2)^2 + F_1(p_1 + ip_2) + F_2 = 0. \quad (\text{A.3})$$

Differentiating with respect to ω , we get

$$2(p_1 + ip_2)(\dot{p}_1 + i\dot{p}_2) + F_1(\dot{p}_1 + i\dot{p}_2) + \dot{F}_1(p_1 + ip_2) + \dot{F}_2 = 0.$$

Comparing the real and imaginary parts from both sides, we have

$$(2p_1 + F_1)\dot{p}_1 - (2p_2)\dot{p}_2 + (\dot{F}_1 p_1 + \dot{F}_2) = 0, \quad (\text{A.4})$$

$$(2p_2)\dot{p}_1 + (2p_1 + F_1)\dot{p}_2 + \dot{F}_1 p_2 = 0. \quad (\text{A.5})$$

Solving we get, $\dot{p}_1 = \frac{-2p_2^2\dot{F}_1 - (2p_1 + F_1)(\dot{F}_1 p_1 + \dot{F}_2)}{(2p_1 + F_1)^2 + 4p_2^2}$.

At, $p_1 = 0$, $p_2 = \pm\sqrt{F_2}$: $\dot{p}_1 = \frac{-2\dot{F}_1 F_2 - F_1 \dot{F}_2}{F_1^2 + 4F_2} \neq 0$. Hence, this completes the proof.

Appendix B

Both the local model (2.5) and the nonlocal model (2.6) show the same dynamics for homogeneous steady states. Let us consider $E^*(u^*, v^*)$ as the coexisting homogeneous steady-state. Now, perturbing the system around (u^*, v^*) by

$$\begin{pmatrix} u \\ v \end{pmatrix} = \begin{pmatrix} u^* \\ v^* \end{pmatrix} + \epsilon \begin{pmatrix} u_1 \\ v_1 \end{pmatrix} e^{\lambda t + ikx}$$

with $|\epsilon| \ll 1$ and substituting these values in system (2.6) the linearization takes the form:

$$\bar{\mathbf{J}}_k \begin{bmatrix} u_1 \\ v_1 \end{bmatrix} \equiv \begin{bmatrix} a_{11} - d_1 k^2 - \lambda & A_{12} \\ a_{21} & a_{22} - d_2 k^2 - \lambda \end{bmatrix} \begin{bmatrix} u_1 \\ v_1 \end{bmatrix} = \begin{bmatrix} 0 \\ 0 \end{bmatrix}, \quad (\text{B.1})$$

where a_{11} , a_{12} , a_{21} and a_{22} are mentioned in the proof of Theorem 3.2 and

$$A_{12} = - \left\{ u^* \frac{\partial f_1}{\partial v} \Big|_{(u^*, v^*)} + \frac{r\omega u^*}{(1 + \omega v^*)^2} \frac{\sin k\delta}{k\delta} \right\} = a_{12} + \frac{r\omega u^*}{(1 + \omega v^*)^2} \left\{ 1 - \left(\frac{\sin k\delta}{k\delta} \right) \right\}.$$

Now, we are interested in finding the non-trivial solution of the system (B.1), so λ must be a zero of $\det(\bar{\mathbf{J}}_k) = 0$, where $\bar{\mathbf{J}}_k$ is the coefficient matrix of the system (B.1). Now

$$\det(\bar{\mathbf{J}}_k) = \lambda^2 - \Gamma(k, d_1, \delta)\lambda + \Delta(k, d_1, \delta),$$

where $\Gamma(k, d_1, \delta) = (a_{11} + a_{22}) - k^2(d_1 + d_2)$ and $\Delta(k, d_1, \delta) = d_1 d_2 k^4 - (a_{11} d_2 + a_{22} d_1) k^2 + (a_{11} a_{22} - a_{21} A_{12})$. So, $\det(\bar{\mathbf{J}}_k) = 0$ will give

$$\lambda(k^2) = \frac{\Gamma(k, d_1, \delta) \pm \sqrt{(\Gamma(k, d_1, \delta))^2 - 4\Delta(k, d_1, \delta)}}{2}.$$

The homogeneous steady-state $E^*(u^*, v^*)$ is stable if $\Gamma(k, d_1, \delta) < 0$ and $\Delta(k, d_1, \delta) > 0$ holds for all k for some fixed d_1 and δ . Now, if the local model is stable, then we already have $\Gamma(k, d_1, \delta) < 0$ here. So, the instability of the coexisting homogeneous steady-state depends on the sign of $\Delta(k, d_1, \delta)$ only. Moreover, Turing instability occurs if $\Gamma(k, d_1, \delta) < 0$ holds for all k and $\Delta(k, d_1, \delta) = 0$ holds for a unique k . $\Gamma(k, d_1, \delta)$ and $\Delta(k, d_1, \delta)$ depending on the parameter δ , and hence it plays an important role for the above instabilities. Therefore, we find these instability conditions by fixing δ . We assume that the equilibrium point E^* is locally asymptotically stable for the temporal model.

To find the condition of Turing instability of the nonlocal model, we need to find a value of d_1 such that $\Delta(k, d_1, \delta) = 0$ for a fixed k and $\Gamma(k, d_1, \delta) < 0$ for all k . Also, for all d_1 , we have got $\Delta(k, d_1, \delta) > 0$ when k is sufficiently small as well as a large quantity. So, $\Delta(k, d_1, \delta) = 0$ holds for a unique k when

$$\Delta(k, d_1, \delta) = 0 \quad \text{and} \quad \frac{\partial \Delta(k, d_1, \delta)}{\partial k} = 0$$

hold, i.e.,

$$d_1 = \frac{d_2 a_{11} k^2 - (a_{11} a_{22} - a_{12} a_{21}) + \frac{a_{21} r \omega u^*}{(1 + \omega v^*)^2} \left(1 - \frac{\sin k\delta}{k\delta} \right)}{k^2 (d_2 k^2 - a_{22})} \quad (\text{B.2a})$$

$$\text{and } 4d_1 d_2 k^3 - 2(d_2 a_{11} + d_1 a_{22})k + \frac{a_{21} r \omega u^*}{k\delta (1 + \omega v^*)^2} \left(\delta \cos k\delta - \frac{\delta \sin k\delta}{k\delta} \right) = 0. \quad (\text{B.2b})$$

From (B.2), eliminating d_1 leads to the following transcendental equation

$$2a_{11} d_2^2 k^4 - 2(2d_2 k^2 - a_{22}) \left[(a_{11} a_{22} - a_{12} a_{21}) - \frac{a_{21} r \omega u^*}{(1 + \omega v^*)^2} \left\{ 1 - \left(\frac{\sin k\delta}{k\delta} \right) \right\} \right] + \frac{a_{21} r \omega u^* (d_2 k^2 - a_{22})}{(1 + \omega v^*)^2} \left(\cos k\delta - \frac{\sin k\delta}{k\delta} \right) = 0, \quad (\text{B.3})$$

which needs to be solved numerically for a fixed value of δ to obtain the critical wave number k_{\min}^T . Here, we may get multiple solutions of (B.3) for a large value of δ . Out of these multiple values of k , we choose k_{\min}^T for which $\Delta(k, d_1, \delta) = 0$ holds for a unique k [see Fig. 6(a)]. Substitution of this value in (B.2a) will give the critical diffusion coefficient $d_{1[c]}^T$. Here $d_1 < d_{1[c]}^T$ leads to $\Delta(k, d_1, \delta) < 0$, so, Turing instability occurs for $d_1 < d_{1[c]}^T$.

References

- [1] S. L. Lima, L. M. Dill, Behavioral decisions made under the risk of predation: a review and prospectus, *Canadian journal of zoology* 68 (4) (1990) 619–640.
- [2] L. Y. Zanette, A. F. White, M. C. Allen, M. Clinchy, Perceived predation risk reduces the number of offspring songbirds produce per year, *Science* 334 (6061) (2011) 1398–1401.
- [3] W. Cresswell, Predation in bird populations, *Journal of Ornithology* 152 (Suppl 1) (2011) 251–263.
- [4] S. D. Peacor, B. L. Peckarsky, G. C. Trussell, J. R. Vonesh, Costs of predator-induced phenotypic plasticity: a graphical model for predicting the contribution of nonconsumptive and consumptive effects of predators on prey, *Oecologia* 171 (2013) 1–10.
- [5] E. L. Preisser, D. I. Bolnick, The many faces of fear: comparing the pathways and impacts of nonconsumptive predator effects on prey populations, *PloS one* 3 (6) (2008) e2465.
- [6] W. J. Ripple, R. L. Beschta, Wolves and the ecology of fear: can predation risk structure ecosystems?, *BioScience* 54 (8) (2004) 755–766.
- [7] A. J. Wirsing, M. R. Heithaus, L. M. Dill, Living on the edge: dugongs prefer to forage in microhabitats that allow escape from rather than avoidance of predators, *Animal Behaviour* 74 (1) (2007) 93–101.
- [8] J. P. Suraci, M. Clinchy, L. M. Dill, D. Roberts, L. Y. Zanette, Fear of large carnivores causes a trophic cascade, *Nature communications* 7 (1) (2016) 10698.
- [9] X. Wang, L. Zanette, X. Zou, Modelling the fear effect in predator–prey interactions, *Journal of mathematical biology* 73 (5) (2016) 1179–1204.
- [10] M. C. Allen, M. Clinchy, L. Y. Zanette, Fear of predators in free-living wildlife reduces population growth over generations, *Proceedings of the National Academy of Sciences* 119 (7) (2022) e2112404119.
- [11] A. J. Gallagher, M. J. Lawrence, S. M. Jain-Schlaepfer, A. D. Wilson, S. J. Cooke, Avian predators transmit fear along the air–water interface influencing prey and their parental care, *Canadian Journal of Zoology* 94 (12) (2016) 863–870.
- [12] R. J. Wootton, *Ecology of teleost fishes*, Vol. 1, Springer Science & Business Media, 2012.
- [13] F. Hua, K. E. Sieving, R. J. Fletcher Jr, C. A. Wright, Increased perception of predation risk to adults and offspring alters avian reproductive strategy and performance, *Behavioral Ecology* 25 (3) (2014) 509–519.
- [14] S. Creel, D. Christianson, S. Liley, J. A. Winnie Jr, Predation risk affects reproductive physiology and demography of elk, *Science* 315 (5814) (2007) 960–960.
- [15] A. J. Wirsing, W. J. Ripple, A comparison of shark and wolf research reveals similar behavioral responses by prey, *Frontiers in Ecology and the Environment* 9 (6) (2011) 335–341.
- [16] M. J. Sheriff, C. J. Krebs, R. Boonstra, The sensitive hare: sublethal effects of predator stress on reproduction in snowshoe hares, *Journal of Animal Ecology* 78 (6) (2009) 1249–1258.
- [17] B. M. Pierce, R. T. Bowyer, V. C. Bleich, Habitat selection by mule deer: forage benefits or risk of predation?, *The Journal of Wildlife Management* 68 (3) (2004) 533–541.
- [18] P. Panday, N. Pal, S. Samanta, J. Chattopadhyay, Stability and bifurcation analysis of a three-species food chain model with fear, *International Journal of Bifurcation and Chaos* 28 (01) (2018) 1850009.
- [19] N. Zhang, Y. Kao, B. Xie, Impact of fear effect and prey refuge on a fractional order prey–predator system with beddington–deangelis functional response, *Chaos: An Interdisciplinary Journal of Nonlinear Science* 32 (4) (2022).

- [20] B. Xie, N. Zhang, Influence of fear effect on a holling type iii prey-predator system with the prey refuge, *AIMS Mathematics* 7 (2) (2022) 1811–1830.
- [21] S. Saha, G. Samanta, Analysis of a tritrophic food chain model with fear effect incorporating prey refuge, *Filomat* 35 (15) (2021) 4971–4999.
- [22] A. A. Thirthar, S. J. Majeed, M. A. Alqudah, P. Panja, T. Abdeljawad, Fear effect in a predator-prey model with additional food, prey refuge and harvesting on super predator, *Chaos, Solitons & Fractals* 159 (2022) 112091.
- [23] H. Zhang, Y. Cai, S. Fu, W. Wang, Impact of the fear effect in a prey-predator model incorporating a prey refuge, *Applied Mathematics and Computation* 356 (2019) 328–337.
- [24] X. Wang, X. Zou, Modeling the fear effect in predator–prey interactions with adaptive avoidance of predators, *Bulletin of mathematical biology* 79 (2017) 1325–1359.
- [25] K. Sarkar, S. Khajanchi, Spatiotemporal dynamics of a predator-prey system with fear effect, *Journal of the Franklin Institute* (2023).
- [26] C. S. Holling, The components of predation as revealed by a study of small-mammal predation of the european pine sawfly1, *The canadian entomologist* 91 (5) (1959) 293–320.
- [27] R. Arditi, H. Akçakaya, Underestimation of mutual interference of predators, *Oecologia* 83 (1990) 358–361.
- [28] P. M. Dolman, The intensity of interference varies with resource density: evidence from a field study with snow buntings, *plectrophenax nivalis*, *Oecologia* 102 (1995) 511–514.
- [29] G. T. Skalski, J. F. Gilliam, Functional responses with predator interference: viable alternatives to the holling type ii model, *Ecology* 82 (11) (2001) 3083–3092.
- [30] J. R. Beddington, Mutual interference between parasites or predators and its effect on searching efficiency, *The Journal of Animal Ecology* (1975) 331–340.
- [31] D. L. DeAngelis, R. Goldstein, R. V. O’Neill, A model for tropic interaction, *Ecology* 56 (4) (1975) 881–892.
- [32] M. W. Group, et al., Diversionary feeding of hen harriers on grouse moors a practical guide, *Scottish Natural Heritage* (1999).
- [33] M. J. Crawley, *Plant ecology*, John Wiley & Sons, 2009.
- [34] G. R. Huxel, K. McCann, G. A. Polis, Effects of partitioning allochthonous and autochthonous resources on food web stability, *Ecological Research* 17 (2002) 419–432.
- [35] P. Srinivasu, B. Prasad, Role of quantity of additional food to predators as a control in predator–prey systems with relevance to pest management and biological conservation, *Bulletin of mathematical biology* 73 (10) (2011) 2249–2276.
- [36] A. M. Turing, The chemical basis of morphogenesis, *Bulletin of mathematical biology* 52 (1990) 153–197.
- [37] M. Banerjee, S. Abbas, Existence and non-existence of spatial patterns in a ratio-dependent predator–prey model, *Ecological Complexity* 21 (2015) 199–214.
- [38] R. E. Wilson, V. Capasso, Analysis of a reaction-diffusion system modeling man–environment–man epidemics, *SIAM Journal on Applied Mathematics* 57 (2) (1997) 327–346.
- [39] G. F. Fussmann, S. P. Ellner, K. W. Shertzer, N. G. Hairston Jr, Crossing the hopf bifurcation in a live predator-prey system, *Science* 290 (5495) (2000) 1358–1360.
- [40] W. Wang, Q.-X. Liu, Z. Jin, Spatiotemporal complexity of a ratio-dependent predator-prey system, *Phys. Rev. E* 75 (2007) 051913.
- [41] M. Banerjee, V. Volpert, Prey-predator model with a nonlocal consumption of prey, *Chaos: An Interdisciplinary Journal of Nonlinear Science* 26 (8) (2016).
- [42] M. Banerjee, V. Volpert, Spatio-temporal pattern formation in rosenzweig–macarthur model: Effect of nonlocal interactions, *Ecological Complexity* 30 (2017) 2–10.
- [43] A. Bayliss, V. Volpert, Complex predator invasion waves in a holling–tanner model with

- nonlocal prey interaction, *Physica D: Nonlinear Phenomena* 346 (2017) 37–58.
- [44] S. Pal, S. Ghorai, M. Banerjee, Analysis of a prey–predator model with non-local interaction in the prey population, *Bulletin of Mathematical Biology* 80 (2018) 906–925.
- [45] R. S. Cantrell, C. Cosner, *Spatial ecology via reaction-diffusion equations*, John Wiley & Sons, 2004.
- [46] S. Pal, M. Banerjee, S. Ghorai, Effects of boundary conditions on pattern formation in a nonlocal prey–predator model, *Applied Mathematical Modelling* 79 (2020) 809–823.
- [47] J. Furter, M. Grinfeld, Local vs. non-local interactions in population dynamics, *Journal of Mathematical Biology* 27 (1989) 65–80.
- [48] L. Perko, *Differential equations and dynamical systems*, Vol. 7, Springer Science & Business Media, 2013.
- [49] S. V. Petrovskii, H. Malchow, Wave of chaos: new mechanism of pattern formation in spatio-temporal population dynamics, *Theoretical population biology* 59 (2) (2001) 157–174.
- [50] S. Petrovskii, B.-L. Li, H. Malchow, Quantification of the spatial aspect of chaotic dynamics in biological and chemical systems, *Bulletin of mathematical biology* 65 (3) (2003) 425–446.
- [51] J. K. Hale, *Theory of functional differential equations*, 2nd Edition, Applied mathematical sciences 3, Springer-Verlag, 1977.